

INFRARED LABORATORY OSCILLATOR STRENGTHS OF Fe I IN THE *H*-BAND

M. P. RUFFONI¹, C. ALLENDE PRIETO², G. NAVE³, AND J. C. PICKERING¹

¹ Blackett Laboratory, Department of Physics, Imperial College London, London SW7 2AZ, UK; m.ruffoni@imperial.ac.uk

² Instituto de Astrofísica de Canarias, E-38205 La Laguna, Tenerife, Spain

³ National Institute of Standards and Technology, Gaithersburg, MD 20899-8422, USA

Received 2013 July 8; accepted 2013 September 12; published 2013 November 19

ABSTRACT

We report experimental oscillator strengths for 28 infrared Fe I transitions, for which no previous experimental values exist. These transitions were selected to address an urgent need for oscillator strengths of lines in the *H*-band (between 1.4 μm and 1.7 μm) required for the analysis of spectra obtained from the Sloan Digital Sky Survey (SDSS-III) Apache Point Galactic Evolution Experiment (APOGEE). Upper limits have been placed on the oscillator strengths of an additional seven transitions, predicted to be significant by published semi-empirical calculations, but not observed to be so.

Key words: atomic data – line: profiles – methods: laboratory: atomic – techniques: spectroscopic

1. INTRODUCTION

In recent years, infrared (IR) spectroscopy has become an important tool for stellar astronomy, as demonstrated by results from the *Spitzer* and *Wide-field Infrared Survey Explorer* (*WISE*) space telescopes, the Cryogenic High-Resolution Infrared Echelle Spectrograph (CRIRES) at the Very Large Telescope, and the Radial Velocity Experiment (RAVE) spectrometer at the Siding Spring Observatory, to name but a few. This research has been made possible by the continual development of better IR detectors for both ground-based and satellite-borne spectrometers; a trend set to continue in the coming decade with the European Space Agency’s (ESA) *Gaia* mission, and planned spectrometers for the European Extremely Large Telescope (E-ELT) facility.

However, during these studies it has become clear that the analysis of expensively acquired astrophysical spectra is often not limited by the capabilities of the spectrometers themselves, but by the lack of accurate reference data in the atomic line database (see, e.g., Boeche et al. 2008; Bigot & Thévenin 2006). One project presently being affected in this way is the Apache Point Galactic Evolution Experiment (APOGEE)—part of the third Sloan Digital Sky Survey (Eisenstein et al. 2011; Allende Prieto et al. 2008; Majewski et al. 2010).

APOGEE is using a highly-multiplexed, near-IR spectrometer (Eisenstein et al. 2011; Wilson et al. 2012), capable of acquiring spectra in the *H*-band (between 1.4 μm and 1.7 μm) from up to 300 stars simultaneously with a spectral resolving power of the order of 30,000. At these wavelengths Galactic dust absorption is more than five times lower than in the optical (e.g., $A_H/A_V = 0.16$), allowing stars in the Galactic bulge and disk to be probed in addition to other stellar populations. During the planned three years of bright time, a homogenous data set of 100,000 stars will be obtained, providing an integrated picture of the chemical and kinematical evolution of the Galaxy (Allende Prieto et al. 2008).

Among the stellar properties being derived from these spectra are the abundances of 15 elements, including Fe peak elements, which will be measured to a precision of 0.1 dex (the unit dex stands for decimal exponent: $x \text{ dex} = 10^x$). A key requirement for such measurements is the availability of accurate oscillator strengths, f (usually used as the $\log(g_l f)$, where g_l is the statistical weight of the lower level), for strong enough, well-resolved lines seen within the *H*-band.

However, in the important case of neutral iron (Fe I), the recent critical compilation of $\log(g_l f)$ s by Fuhr & Wiese (2006) listed only the 51 transitions of O’Brian et al. (1991) with a wavelength greater than 1 μm ; grading them C to D+, indicating uncertainties in $\log(g_l f)$ of 25%–50%.

This inadequacy is at least in part due to the difficulty in measuring $\log(g_l f)$ s in the IR. Typically, oscillator strengths are obtained in the laboratory from measurements of atomic transition probabilities, A (Thorne et al. 2007a).

$$\log(g_l f) = \log[A_{ul} g_u \lambda^2 \times 1.499 \times 10^{-14}], \quad (1)$$

where the subscript u denotes a target upper energy level, and ul , a transition from this level to a lower state, l , which results in the emission of photons of wavelength λ (nm). g_u is the statistical weight of the upper level. The A_{ul} values are found by combining experimental branching fractions, BF_{ul} , with radiative lifetimes, τ_u (Huber & Sandeman 1986):

$$A_{ul} = \frac{\text{BF}_{ul}}{\tau_u}; \quad \tau_u = \frac{1}{\sum_l A_{ul}}. \quad (2)$$

The BF_{ul} are commonly obtained from the ratio of calibrated emission line intensities, measured, for example, with Fourier transform (FT) spectrometry (Pickering et al. 2001). This was the technique adopted in this study, and is described in more detail in Section 2.1. However, for reliable line intensity calibration, all emission lines from an upper level must be sufficiently closely spaced in wavenumber to either be observed in a single spectrum, or be seen in a number of overlapping spectra where at least one line from the target upper level is present in the overlap region to carry the intensity calibration from one spectrum to the next.

τ_u is usually measured with time-resolved laser induced fluorescence (LIF). In a typical LIF experiment, such as that reported by O’Brian et al. (1991) and Engelke et al. (1993), an atomic beam of the target material is generated by a hollow-cathode discharge lamp (HCL), and is then excited by a light pulse from a pumped dye laser, the frequency of which is tunable in the visible to UV range. For a target upper level to be populated by this pulse, a strong transition must exist between it and an already populated lower level, where the energy difference matches that of the laser light.

However, when studying IR transitions, the requirements for each of these two experiments often become mutually exclusive.

Table 1
FT Spectra Recorded for the BF Measurements

Tag	Wavenumber Range (cm ⁻¹)	Carrier Gas and Pressure (mbar)	Current (A)	Spectrum Filename(s) ^a
A	1800–15000	Ne, 3.7	2.0	Fe072511.002 to .010; Fe072611.006 to .012; Fe072711.002 to .005
B	1800–15000	Ne, 3.7	1.4	Fe072511.001
C	1800–15000	Ar, 2.7	2.0	Fe072201.001 to .004

Notes. All spectra were measured with InSb detectors on the 2 m FT spectrometer at NIST.

^a Where more than one filename is given, the named spectra were coadded to improve the signal-to-noise ratio of weak lines.

BFs can be obtained for transitions from upper levels that only produce closely spaced IR lines, but since these levels are relatively highly excited, they are not easily populated in a LIF experiment. Conversely, LIF measurements can be performed on upper levels that include at least one transition to a populated low-lying state, but because such a transition would usually be seen in the ultraviolet, a large gap would be present between it and any IR lines, preventing emission spectra acquired in the two regions from being placed on a common intensity scale.

In identifying the Fe I transitions that will be required for the analysis of APOGEE spectra, we have found that the former situation typically prevails. We have therefore measured BFs in the normal way (Pickering et al. 2001), as described in Section 2.1, but have been forced to seek alternative means of normalizing them to obtain the required transition probabilities from Equation (2).

In Section 2.4, we describe a method for obtaining “effective lifetimes” for target upper levels by refining the semi-empirical lifetimes of Kurucz (2007). Transition probabilities obtained with reference to these effective lifetimes are then examined further in Section 2.5, where we employ the long-established Ladenburg technique to obtain *relative* $\log(g_l f)$ s from networks of interconnected transitions without prior knowledge of the associated upper level lifetimes (Ladenburg 1933).

Results obtained from each of these two methods are then presented in Section 3, where we also provide recommended $\log(g_l f)$ values for the most critical Fe I transitions needed for the APOGEE project. Further transitions of interest to APOGEE (and complementary projects, such as *Gaia*-ESO) will be published in the near future.

2. EXPERIMENTAL PROCEDURE

2.1. Branching Fraction Measurements

The BF of a given transition from upper level, u , is the ratio of its A_{ul} to the sum of all A_{ul} associated with u . Given an intensity calibrated line spectrum, this is equivalent to the ratio of observed relative line intensities for these transitions:

$$\text{BF}_{ul} = \frac{A_{ul}}{\sum_l A_{ul}} = \frac{I_{ul}}{\sum_l I_{ul}}. \quad (3)$$

This approach does not depend on any form of equilibrium in the population distribution over different levels, but it is essential that all significant transitions from u be included in the sum over l .

The BFs reported here were obtained from Fe I atomic emission line spectra measured between 1800 cm⁻¹ and 25,000 cm⁻¹ (between 5555 nm and 400 nm) on the 2 m FT spectrometer at the National Institute of Standards and Technology (NIST; Nave et al. 1997). The spectrum was excited from a 99.8% pure Fe cathode mounted in a water cooled HCL running under the conditions shown in Table 1. All the results reported in Section 3

were obtained from spectrum A, with spectra B and C being used to check that the target lines were free from self-absorption or blends with carrier gas lines.

The intensity of each spectrum was calibrated using a tungsten (W) halogen lamp with spectral radiance known to $\pm 1.1\%$ between 250 nm and 6000 nm. Spectra of this lamp were recorded both before and after the acquisition of each Fe spectrum using the same spectrometer parameters, and the measured intensity used to obtain the spectrometer response function. The full procedure is discussed in detail by Pickering et al. (2001). The number of Fe scans taken between each W lamp spectrum was limited to ensure all three spectra (W, Fe, W) could be acquired within approximately 2 hr. Over this period, negligible variation in spectrometer response was observed. The two W lamp spectra were thus co-added and the resulting spectrum was used to obtain the spectrometer response function, from which the Fe spectrum was intensity calibrated.

Where additional Fe scans were required to increase the signal-to-noise ratio (S/N) of target transitions, multiple sets of W, Fe, W spectra were obtained, and each of the calibrated Fe spectra were co-added to produce a single composite spectrum.

2.2. Line Fitting

For each target upper level, the semi-empirical calculations of Kurucz (2007) were used to give a list of predicted transitions to lower levels, as shown diagrammatically in Figure 1. The emission lines of these transitions were then identified in our Fe spectra, and the XGremLin package (Nave et al. 1997) was used to obtain relative line intensities by fitting Voigt profiles to them. Some lines, predicted by Kurucz to contribute less than 1% to the total BF, were too weak to be observed. The sum total of their predicted BFs was thus assigned to an unobserved “residual.” This was then included in the summation over l in Equation (3) to normalize the sum of all BFs to unity. BFs and $\log(g_l f)$ s were obtained with the aid of the FAST package (Ruffoni 2013).

In some cases, there was disagreement between the predicted intensity of a line and that observed experimentally. Where lines were predicted to be visible above our experimental noise limit, but were absent in our spectra, we assigned a maximum possible BF to each unobserved line, based on the noise at its expected wavenumber. These disagreements were associated with transitions from $4f$ upper levels, and would likely be due to a high degree of level mixing, lowering the accuracy of predicted line intensities.

2.3. Uncertainties in Branching Fractions and $\log(g_l f)$ s

Several sources of uncertainty contributed to the overall uncertainty in the intensity of a given line:

1. The uncertainty in the intensity of the line profile, obtained from the inverse of its S/N.

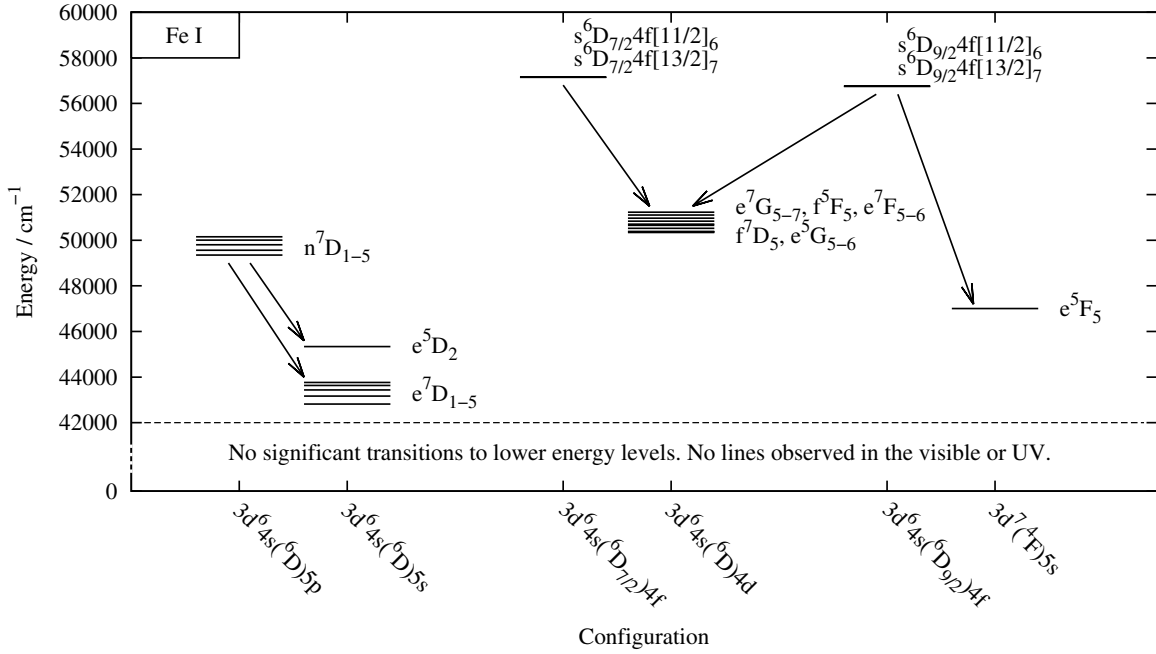


Figure 1. Fe I upper energy levels for which branching fractions to the indicated lower levels were measured. Each level, or collection of levels where they are close together in energy, is labeled with its term and grouped with others of the same configuration.

2. The uncertainty in the intensity of the tungsten standard lamp when measured on the FT spectrometer, obtained from the inverse of its S/N at the same wavenumber as the line.
3. The uncertainty in the calibrated spectral radiance of the tungsten lamp at the same wavenumber as the line. Within one spectrum we ascribe $1/\sqrt{2}$ of the quoted one standard deviation lamp calibration error, ϵ , to each line so that the uncertainty in the intensity ratio of any two lines is ϵ .

These are added in quadrature to give an overall uncertainty in the calibrated intensity of a given line profile, ΔI_{ul} . Uncertainties in individual BFs, $\Delta(\text{BF})_{ul}$, are then given by

$$\left(\frac{\Delta(\text{BF})_{ul}}{(\text{BF})_{ul}}\right)^2 = (1 - 2(\text{BF})_{ul}) \left(\frac{\Delta I_{ul}}{I_{ul}}\right)^2 + \sum_{j=1}^n (\text{BF})_{uj}^2 \left(\frac{\Delta I_{uj}}{I_{uj}}\right)^2. \quad (4)$$

This formalism is derived from Equation (7) in Sikström et al. (2002), and takes special account of the correlation between I_{ul} and $\sum_l I_{ul}$ that arises from the presence of a given line intensity in both the numerator and denominator on the right-hand side of Equation (3). The uncertainty in the transition probability of a given line, ΔA_{ul} , is then

$$\left(\frac{\Delta A_{ul}}{A_{ul}}\right)^2 = \left(\frac{\Delta(\text{BF})_{ul}}{(\text{BF})_{ul}}\right)^2 + \left(\frac{\Delta \tau_{ul}}{\tau_{ul}}\right)^2, \quad (5)$$

where $\Delta \tau_{ul}$ is the uncertainty in upper level lifetime. This then leads to the uncertainty in $\log(g_l f)$ of a given line,

$$\Delta \log(g_l f)(\text{dex}) = \log \left[g_l f \left(1 + \frac{\Delta A_{ul}}{A_{ul}} \right) \right] - \log[g_l f]. \quad (6)$$

2.4. Determining Effective Radiative Lifetimes

Upper level radiative lifetimes are typically obtained from LIF measurements, as described in Section 1. However, this

Table 2
Radiative Lifetimes for Fe I Levels Linked to Transitions
of High Importance to APOGEE

Configuration	Term	J	Energy (cm^{-1})	Lifetime, τ (ns)	
				Theory ^a	Effective ^b
$3d^6 4s(6D)5p$	n^7D	5	49352.338	71.429	97 ± 12
	n^7D	4	49558.731	69.930	101 ± 14
	n^7D	3	49805.254	68.027	95 ± 12
	n^7D	2	50008.519	68.493	94 ± 14
	n^7D	1	50152.616	71.429	89 ± 11
$3d^6 4s(6D_{7/2})4f$	$s^6D_{3.54f}[5.5]$	6	57146.768	55.249	67 ± 9
	$s^6D_{3.54f}[6.5]$	7	57152.331	56.818	69 ± 18
$3d^6 4s(6D_{9/2})4f$	$s^6D_{4.54f}[5.5]$	6	56748.897	46.512	41 ± 6
	$s^6D_{4.54f}[6.5]$	7	56754.128	54.945	54 ± 7

Notes. The configuration, term, and energy level data are taken from Nave et al. (1994).

^a Semi-empirical values calculated by Kurucz (2007).

^b The uncertainty in effective lifetimes includes the 0.05 dex uncertainty in the solar Fe abundance of Asplund et al. (2005).

technique cannot be applied to the levels studied here, forcing us to adopt a different approach.

Table 2 lists the upper levels from which we wish to find the $\log(g_l f)$ s of transitions to lower levels. The Theory column shows the upper level lifetimes calculated by Kurucz (2007). These were combined with our experimental BFs to arrive at an initial estimate to the $\log(g_l f)$ of each transition listed in Table 3. These $\log(g_l f)$ s were then used in conjunction with a one-dimensional (1D) model atmosphere interpolated from the calculations by Castelli & Kurucz (2004) for the atmospheric parameters of the Sun ($T_{\text{eff}} = 5777$ K, $\log(\text{gravity in cm s}^{-2}) = 4.437$) to generate synthetic Fe I spectral lines, which were then compared with the solar spectrum from the atlas by Livingston & Wallace (1991; see also Wallace et al. 1996). This solar atlas was obtained with the Fourier Transform Spectrograph formerly

Table 3
Effective Upper Level Lifetimes Found for Individual Transitions in Stellar Spectra

Upper Level (u)	Lower Level (l)	Transition ^a		Initial $\log(g_l f)$	Stellar $\delta \log(g_l f)$	VdW Broadening ($\text{rad s}^{-1} \text{cm}^3$)	Effective τ_u (ns)
		Air λ_{ul} (nm)	σ_{ul} (cm^{-1})				
$n^7 D_5$	$e^7 D_4$	1615.3249	6189.014	-0.529	-0.149	-6.97	101 ± 4
	$e^7 D_5$	1529.4562	6536.485	0.710	-0.117	-7.21	94 ± 4
$n^7 D_4$	$e^7 D_3$	1632.4459	6124.104	-0.414	-0.136	-6.96	94 ± 8
	$e^7 D_4$	1563.1950	6395.407	0.186	-0.201	-6.96	109 ± 8
$n^7 D_3$	$e^7 D_2$	1619.8505	6171.723	-0.317	-0.156	-6.95	97 ± 3
	$e^7 D_3$	1569.2751	6370.628	-0.369	-0.133	-6.95	92 ± 3
$n^7 D_2$	$e^7 D_1$	1600.9615	6244.540	-0.375	-0.114	-6.95	91 ± 14
	$e^7 D_2$	1568.2021	6374.987	-2.200	-0.036	-7.15	76 ± 20
$n^7 D_1$	$e^7 D_3$	1520.7530	6573.893	0.307	-0.192	-7.02	109 ± 14
	$e^7 D_1$	1564.8515	6388.637	-0.516	-0.103	-6.78	91 ± 2
	$e^7 D_2$	1533.5387	6519.084	0.070	-0.090	-7.07	88 ± 1
$s^6 D_{3,5}4f[5.5]_6$	$f^5 F_5$	1654.1968	6043.579	-0.253	-0.087	-6.75	68 ± 5
	$e^7 G_6$	1617.9585	6178.940	0.227	-0.106	-6.75	71 ± 3
	$e^7 F_5$	1583.5164	6313.334	0.790	-0.054	-7.01	63 ± 3
$s^6 D_{3,5}4f[6.5]_7$	$e^7 G_6$	1616.5031	6184.503	0.969	-0.170	-6.78	84 ± 16
	$e^7 F_6$	1467.9844	6810.200	-0.137	0.032	-6.80	53 ± 16
$s^6 D_{4,5}4f[5.5]_6$	$e^5 G_5$	1653.8000	6045.029	-0.639	0.096	-6.89	37 ± 7
	$e^7 G_7$	1639.6311	6097.267	-0.683	0.099	-6.80	37 ± 7
	$f^7 D_5$	1569.1857	6370.991	0.543	0.005	-6.80	46 ± 4
$s^6 D_{4,5}4f[6.5]_7$	$e^7 G_7$	1638.2256	6102.498	0.342	0.000	-6.80	55 ± 2
	$e^7 F_6$	1559.1497	6412.000	0.887	0.020	-7.00	53 ± 1

Note. ^a Transition wavenumber and air wavelength data from Nave et al. (1994).

at the Pierce-McMath facility at Kitt Peak National Observatory, with a resolving power $R \sim 300,000$.

The spectral synthesis calculations were performed with the ASS ϵ T code (Koesterke et al. 2008; Koesterke 2009). We would have liked to have obtained an optimized solar iron abundance from fits to Fe I H -band lines with known, accurate $\log(g_l f)$ s. However, as already stated in the motivation for this study, such data are not available. In their absence, we adopted the solar abundance of $7.45 \pm 0.05 \text{ dex}^4$ from Asplund et al. (2005). Although this value was obtained by those authors through the use of a three-dimensional (3D) stellar atmosphere code, 3D effects on Fe I lines in the Sun are known to be small (Asplund et al. 2000; Allende Prieto et al. 2002). Furthermore, other recent solar studies using 1D model atmospheres, have produced Fe abundances in agreement with this value (Ramírez et al. 2013).

We made use of the most complete line list available to us, including both atomic and molecular transitions (M. Shetrone 2013, private communication), which facilitates the analysis of Fe I lines in the vicinity of other transitions. Radiative and Stark damping constants were adopted from the Kurucz Web site, and Van der Waals (VdW) while damping constants (collisional damping due to neutral atoms) were taken from Meléndez & Barbay (1999) when available (calculated from the tables by Anstee & O’Mara 1995, Barklem & O’Mara 1997, and Barklem et al. 1998) and slightly adjusted to match the solar spectrum (M. Shetrone 2013, in preparation).

A micro-turbulence of 1.1 km s^{-1} was included in the radiative transfer calculations. Each model spectrum was convolved with a Gaussian with a FWHM of 2.3 km s^{-1} to account for the instrumental profile (FWHM $\sim 1 \text{ km s}^{-1}$) and, most importantly, macro-turbulence. The adopted macro-turbulence is smaller than the values typically found in the optical (see, e.g., Allende Prieto et al. 2001). Such difference is likely related to

the Fe I IR lines forming in a different range of atmospheric layers than Fe I optical lines, due to the lower continuum opacity in the H band. Wavelength offsets were removed (since it was line intensities that were of interest), and the background continuum level adjusted when necessary. The intensity of each model line, I_{model} , was then compared to the corresponding line intensity observed, I_{obs} , and our initial $\log(g_l f)$ varied until the two were matched. This provided a $\log(g_l f)$ correction factor, $\delta \log(g_l f)$, for each line.

Figure 2 shows two examples of the fitted line profiles. Our refined synthetic profile is plotted as a dashed black line and the observed solar profile as a solid black line. The remaining solid and dashed gray plots show the change in I_{model} for successive ± 0.1 offsets to our initial $\log(g_l f)$. The cross-hatched gray area around each line shows the region used to compare the model and observed spectra. Its width was chosen to avoid neighboring lines, and its height was restricted to relative fluxes between 0.7 and 1.0 to limit the influence of possible non-local thermodynamic equilibrium (NLTE) effects. NLTE effects tend to be most important in the outermost, low-density atmospheric layers, and therefore affect most significantly the cores of strong lines. The inset in each plot shows the sum of differences in relative flux $(I_{\text{obs}} - I_{\text{model}})^2$ as a function of $\delta \log(g_l f)$, where the dashed vertical line indicates the optimal value of $\delta \log(g_l f)$, obtained from the minimum of a parabolic fit to the differences at each $\delta \log(g_l f)$. Table 3 lists all the lines for which refined $\log(g_l f)$ s were determined.

If it is assumed that each $\delta \log(g_l f)$ is due to an error in the corresponding Kurucz upper level lifetime, rather than any other source, it can be directly related to a correction in τ_u . By adding each $\delta \log(g_l f)$ to its initial experimental $\log(g_l f)$ and determining the corresponding value of A_{ul} , Equation (2) can be inverted to obtain an improved estimate of the upper level lifetime, as listed in Table 3. Averaging these values over all lines belonging to a given upper level then provides a refined value of

⁴ On the usual logarithmic abundance scale, where the hydrogen abundance is 12.00 by definition.

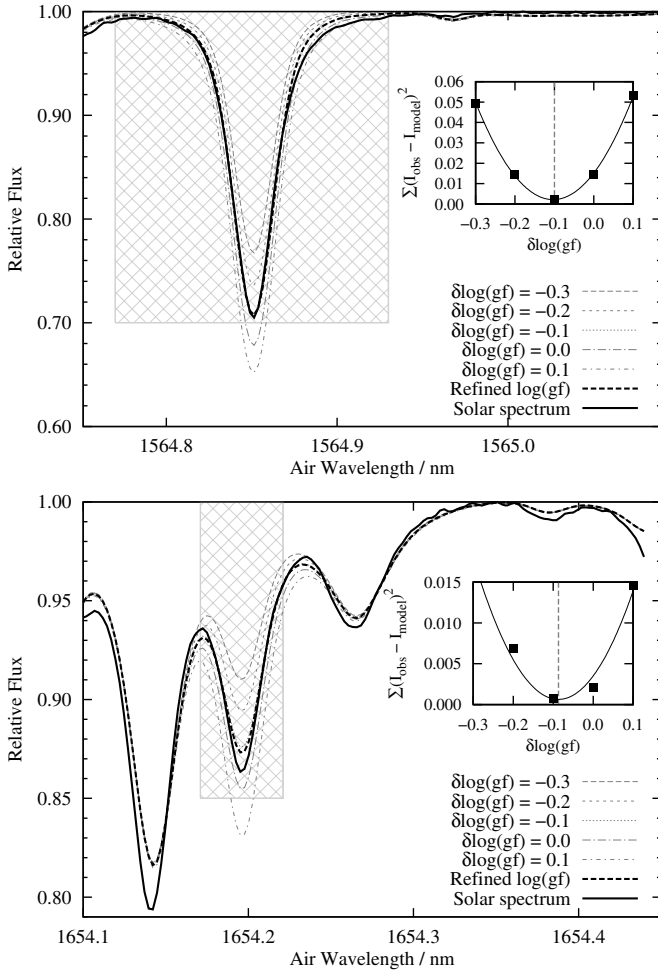


Figure 2. Determining $\delta \log(g_i f)$ s from fits of modeled line profiles to stellar spectra.

τ_u for that level, as listed in Table 2 in the “Effective Lifetime” column. These were then combined with our experimentally measured BFs to provide refined $\log(g_i f)$ s for all lines from each target upper level, as described in Section 3 and listed in the “BF & Effective τ ” column in Table 6.

The uncertainties in the individual lifetimes shown in Table 3 were estimated by combining the uncertainty in the BF (and thus intensity) for the line, the uncertainty in determining $\delta \log(g_i f)$, and the standard deviation of refined lifetimes for all lines

belonging to the same upper level. When these were combined to provide the uncertainties in effective lifetimes listed in Table 2, an additional uncertainty of 12% was included to account for the 0.05 dex uncertainty in solar Fe abundance quoted by Asplund et al. (2005).

This uncertainty in solar Fe abundance significantly increased the overall uncertainty in the effective lifetimes. Nonetheless, the refinement procedure reduced the probable error in each lifetime from approximately 20% or more, found by taking the median difference between the Kurucz (2007) lifetimes and experimental values for the levels studied in O’Brian et al. (1991) and Engelke et al. (1993), to between 12% and 15%.

2.5. Verifying the Refined $\log(g_i f)$ s Using the Ladenburg Technique

Given the non-standard approach we have been forced to adopt to obtain effective upper level lifetimes, the accuracy of the refined $\log(g_i f)$ s described in Section 2.4 must be examined further.

Relative $\log(g_i f)$ s can be obtained for a set of transitions originating from a common upper or lower level by comparing their relative calibrated line intensities (Huber & Sandeman 1986; Thorne et al. 2007b; Ladenburg 1933). When these line intensities are measured in emission, upper level branching ratios are obtained, which are similar to the BFs described in Section 2.1, but do not necessarily include all significant transitions from u to l . When measured in absorption, relative $\log(g_i f)$ s can be found for transitions to different upper levels that share a common lower level. Thus, a network of linked upper and lower levels may be formed. The relative $\log(g_i f)$ s of all the interconnecting transitions are placed on an absolute scale by finding the absolute $\log(g_i f)$ of any one transition.

While the accuracy of these $\log(g_i f)$ s relies on the accuracy of the chosen reference $\log(g_i f)$, this approach has the advantage that not all transitions down from an upper level, or up from a lower level, must be included in the network. Furthermore, and most importantly from the perspective of verifying the accuracy of the refined $\log(g_i f)$ s reported in Table 6, no knowledge of the upper level lifetime is required.

Figure 3 shows the transitions that link the five n^7D upper levels studied here. The effective lifetimes for the two transitions from n^7D_1 show the best consistency in Table 3, with the transition from n^7D_1 to e^7D_1 also exhibiting the smallest $\delta \log(g_i f)$ after refining the Kurucz lifetime. We therefore asserted that its refined experimental $\log(g_i f)$ is a good representation of

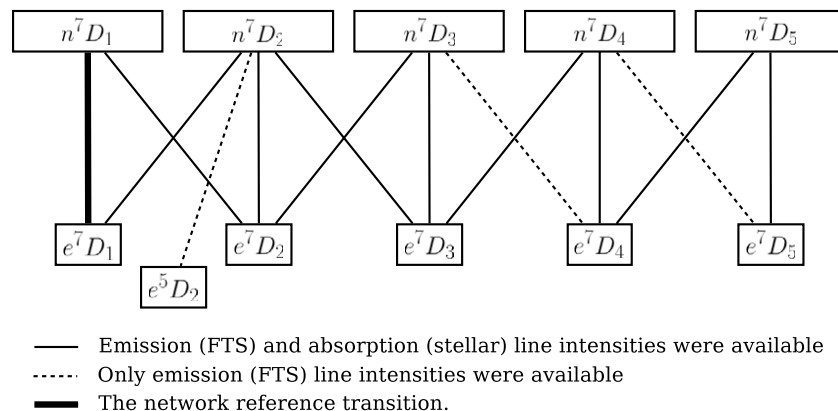


Figure 3. Network of transitions that link the studied n^7D upper levels.

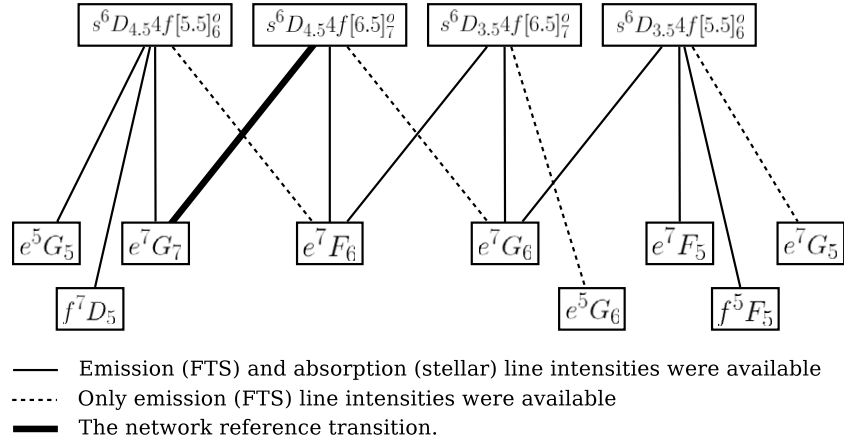

Figure 4. Network of transitions that link the studied 4f upper levels.

Table 4
 The Network of Linked Transitions Stemming from the $n^7 D_1$ to $e^7 D_1$ Transition

Upper Level (u)	Lower Level (l)	Transition		Emission I (arb. unit)	Absorption I (arb. unit)	Transfer Ratio
		Air λ_{ul} (nm)	σ_{ul} (cm^{-1})			
$n^7 D_5$	$e^7 D_4$	1615.3249	6189.014	8.765×10^3	4.879×10^5	$n^7 D_5/n^7 D_4$
	$e^7 D_5$	1529.4562	6536.485	1.696×10^5		$e^7 D_5/e^7 D_4$
$n^7 D_4$	$e^7 D_3$	1632.4459	6124.104	1.036×10^4	7.679×10^5	$n^7 D_4/n^7 D_3$
	$e^7 D_4$	1563.1950	6395.407	4.499×10^4	2.930×10^6	$e^7 D_4/e^7 D_3$
$n^7 D_3$	$e^7 D_5$	1482.6412	6742.877	8.356×10^4		$e^7 D_5/e^7 D_3$
	$e^7 D_2$	1619.8505	6171.723	1.229×10^4	1.223×10^6	$n^7 D_3/n^7 D_1$
$n^7 D_2$	$e^7 D_3$	1569.2751	6370.628	1.162×10^4	1.218×10^6	$e^7 D_3/e^7 D_2$
	$e^7 D_4$	1505.1749	6641.931	7.555×10^4		$e^7 D_4/e^7 D_2$
$n^7 D_1$	$e^5 D_2$	2138.6166	4674.644	2.589×10^2		$e^5 D_2/e^7 D_1$
	$e^7 D_1$	1600.9615	6244.540	1.060×10^4	1.688×10^6	$n^7 D_2/n^7 D_1$
$n^7 D_1$	$e^7 D_2$	1568.2021	6374.987	1.653×10^2		$e^7 D_2/e^7 D_1$
	$e^7 D_3$	1520.7530	6573.893	5.652×10^4		$e^7 D_3/e^7 D_1$
$n^7 D_1$	$e^7 D_1$	1564.8515	6388.637	7.520×10^3	2.184×10^6	Fixed
	$e^7 D_2$	1533.5387	6519.084	3.020×10^4	9.030×10^6	$e^7 D_2/e^7 D_1$

Table 5
 The Network of Linked Transitions Stemming from the $s^6 D_{4.5} 4f [6.5]_7$ to $e^7 G_7$ Transition

Upper Level (u)	Lower Level (l)	Transition		Emission I (arb. unit)	Absorption I (arb. unit)	Transfer Ratio
		Air λ_{ul} (nm)	σ_{ul} (cm^{-1})			
$s^6 D_{3.5} 4f [6.5]_7$	$e^7 G_6$	1616.5031	6184.503	1.948×10^4	1.232×10^7	$e^7 G_6/e^7 F_6$
	$e^5 G_6$	1508.0225	6629.389	2.695×10^2		$e^5 G_6/e^7 F_6$
$s^6 D_{4.5} 4f [6.5]_7$	$e^7 F_6$	1467.9844	6810.200	1.847×10^3	1.285×10^6	$s^6 D_{3.5} 4f [6.5]_7/s^6 D_{4.5} 4f [6.5]_7$
	$e^7 G_6$	1727.7482	5786.300	5.194×10^2		$e^7 G_6/e^7 G_7$
$s^6 D_{4.5} 4f [5.5]_6$	$e^7 G_7$	1638.2256	6102.498	4.718×10^3	3.642×10^6	Fixed
	$e^7 F_6$	1559.1497	6412.000	1.829×10^4	1.477×10^7	$e^7 F_6/e^7 G_7$
$s^6 D_{4.5} 4f [5.5]_6$	$e^5 G_5$	1653.8000	6045.029	5.575×10^2		$e^5 G_5/e^7 G_7$
	$e^7 G_7$	1639.6311	6097.267	5.129×10^2	4.978×10^5	$s^6 D_{4.5} 4f [5.5]_6/s^6 D_{4.5} 4f [6.5]_7$
$s^6 D_{3.5} 4f [5.5]_6$	$f^7 D_5$	1569.1857	6370.991	9.423×10^3		$f^7 D_5/e^7 G_7$
	$e^7 F_6$	1560.4225	6406.770	1.263×10^4		$e^7 F_6/e^7 G_7$
$s^6 D_{3.5} 4f [5.5]_6$	$e^7 G_5$	1689.2375	5918.214	5.409×10^2		$e^7 G_5/e^7 G_6$
	$f^5 F_5$	1654.1968	6043.579	1.024×10^3		$f^5 F_5/e^7 G_6$
$s^6 D_{3.5} 4f [5.5]_6$	$e^7 G_6$	1617.9585	6178.940	3.230×10^3	2.591×10^6	$s^6 D_{3.5} 4f [5.5]_6/s^6 D_{3.5} 4f [6.5]_7$
	$e^7 F_5$	1583.5164	6313.334	1.232×10^4		$e^7 F_5/e^7 G_6$

the absolute $\log(g_l f)$ that would have been obtained if τ_l were known. This was thus the reference transition against which we measured relative $\log(g_l f)$ s of all the other transitions in the network.

Table 4 lists the calibrated line intensities for this network of transitions, measured in both emission, with FT spectroscopy, and absorption from our synthetic line profile fits to the solar

spectrum of Livingston & Wallace (1991). The $\log(g_l f)$ of the $n^7 D_1$ to $e^7 D_1$ transition was fixed to the refined value listed in Table 6. The Transfer Ratio column of Table 6 shows which two levels were used to link this $\log(g_l f)$ to others in the network. Where this ratio was between two lower levels in the network, the transfer was made using the ratio of emission line intensities from a common upper level. Where it was between two upper

Table 6
Experimental Branching Fractions, Transition Probabilities, and $\log(g_l f)$ s for the Fe I Levels Listed in Table 2

Upper Level (u)	Lower Level (l)	Transition ^a		BF	Δ BF (%)	A_{ul} (10^6 s^{-1})	BF & Effective τ		Ladenburg		Recommended	
		Air λ_{ul} (nm)	σ_{ul} (cm^{-1})				$\log(g_l f)$	\pm dex	$\log(g_l f)$	\pm dex	$\log(g_l f)$	\pm dex
$n^7 D_5$	$e^7 D_4$	1615.3249	6189.014	0.049	1.29	0.506	-0.66	0.05	-0.65	0.06	-0.66	0.05
	$e^7 D_5$	1529.4562	6536.485	0.950	0.07	9.795	0.58	0.05	0.59	0.06	0.58	0.05
		Residual			0.001							
$n^7 D_4$	$e^7 D_3$	1632.4459	6124.104	0.073	1.12	0.727	-0.58	0.06	-0.59	0.05	-0.59	0.05
	$e^7 D_4$	1563.1950	6395.407	0.319	0.72	3.156	0.02	0.06	0.01	0.05	0.01	0.05
	$e^7 D_5$	1482.6412	6742.877	0.592	0.42	5.862	0.24	0.06	0.24	0.05	0.24	0.05
		Residual			0.016							
$n^7 D_3$	$e^7 D_2$	1619.8505	6171.723	0.119	1.02	1.254	-0.46	0.05	-0.48	0.05	-0.46	0.05
	$e^7 D_3$	1569.2751	6370.628	0.113	1.18	1.185	-0.51	0.05	-0.53	0.05	-0.51	0.05
	$e^7 D_4$	1505.1749	6641.931	0.732	0.27	7.708	0.26	0.05	0.25	0.05	0.26	0.05
		Residual			0.036							
$n^7 D_2$	$e^5 D_2$	2138.6166	4674.644	0.004	24.6	0.040	-1.86	0.11	-1.84	0.11	-1.84	0.11
	$e^7 D_1$	1600.9615	6244.540	0.154	1.04	1.634	-0.50	0.06	-0.48	0.05	-0.48	0.05
	$e^7 D_2$	1568.2021	6374.987	0.002	18.6	0.025	-2.33	0.09	-2.31	0.09	-2.31	0.09
	$e^7 D_3$	1520.7530	6573.893	0.819	0.23	8.711	0.18	0.06	0.20	0.05	0.20	0.05
		Residual			0.021							
$n^7 D_1$	$e^7 D_1$	1564.8515	6388.637	0.198	1.18	2.222	-0.61	0.05	-0.61	0.05	-0.61	0.05
	$e^7 D_2$	1533.5387	6519.084	0.794	0.30	8.925	-0.03	0.05	-0.03	0.05	-0.03	0.05
	Residual			0.008								
$s^6 D_{3,5}4f[5.5]_6$	$e^7 G_5$	1689.2375	5918.214	0.031	15.0	0.457	-0.60	0.08	-0.59	0.08	-0.60	0.08
	$f^5 F_5$	1654.1968	6043.579	0.058	6.20	0.865	-0.34	0.06	-0.33	0.06	-0.34	0.06
	$e^7 G_6$	1617.9585	6178.940	0.183	1.68	2.727	0.14	0.06	0.15	0.06	0.14	0.06
	$e^7 F_5$	1583.5164	6313.334	0.697	0.81	10.396	0.71	0.05	0.71	0.06	0.71	0.05
	$f^7 D_5$	1476.9493	6768.863	<0.008 ^c		0.120	-1.29	0.16			-1.29	0.16
	Residual			0.023								
$s^6 D_{3,5}4f[6.5]_7$	$e^7 G_6$	1616.5031	6184.503	0.901	0.64	12.692	0.87	0.10	0.89	0.05	0.89	0.05
	$e^5 G_6$	1508.0225	6629.389	0.012	32.6	0.176	-1.05	0.15	-1.03	0.13	-1.03	0.13
	$e^7 F_6$	1467.9844	6810.200	0.085	5.27	1.204	-0.23	0.10	-0.22	0.05	-0.22	0.05
		Residual			0.002							
$s^6 D_{4,5}4f[5.5]_6$	$e^7 G_5$	<i>1810.986</i>	<i>5520.347^b</i>	<0.001 ^c		0.013	-2.09	0.82			-2.09	0.82
	$f^7 F_5$	1770.7734	5645.708	<0.005 ^c		0.131	-1.10	0.11			-1.10	0.11
	$e^7 F_5$	1690.0234	5915.462	<0.004 ^c		0.091	-1.30	0.26			-1.30	0.26
	$e^5 G_5$	1653.8000	6045.029	0.020	14.0	0.489	-0.58	0.08	-0.53	0.08	-0.53	0.08
	$e^7 G_7$	1639.6311	6097.267	0.018	16.4	0.450	-0.63	0.09	-0.58	0.05	-0.58	0.05
	$e^5 G_6$	<i>1605.740</i>	<i>6225.956^b</i>	<0.003 ^c		0.063	-1.50	0.28			-1.50	0.28
	$f^7 D_5$	1569.1857	6370.991	0.339	1.80	8.261	0.60	0.06	0.65	0.06	0.65	0.06
	$e^7 F_6$	1560.4225	6406.770	0.454	1.77	11.068	0.72	0.06	0.77	0.06	0.77	0.06
	$e^5 F_5$	<i>1026.055</i>	<i>9743.394^b</i>	<0.001 ^c		0.013	-2.56	1.28			-2.56	1.28
	$a^5 F_5$	200.655	49820.629	0.152 ^d								
	Residual			0.003								
$s^6 D_{4,5}4f[6.5]_7$	$e^7 G_6$	1727.7482	5786.300	0.022	20.0	0.408	-0.56	0.09	-0.56	0.09	-0.56	0.09
	$e^7 G_7$	1638.2256	6102.498	0.200	1.92	3.704	0.35	0.05	0.35	0.05	0.35	0.05
	$e^5 G_6$	<i>1604.392</i>	<i>6231.187^b</i>	<0.002 ^c		0.037	-1.67	0.18			-1.67	0.18
	$e^7 F_6$	1559.1497	6412.000	0.776	0.67	14.362	0.90	0.05	0.90	0.05	0.90	0.05
	Residual			<0.001								

Notes. The Residual BF is the sum total BF of all other lines predicted by Kurucz for the given upper level, but which were either outside the measurement range or predicted to contribute less than 1% of the total BF.

^a Transition wavenumber and air wavelength data from Nave et al. (1994).

^b Nave et al. (1994) did not detect these lines. Transition data shown is from Kurucz (2007).

^c Kurucz predicts these transitions have BF's of at least 1%, yet they are unobserved in our spectra. For each transition, the quoted wavelength and wavenumber (in italics) are therefore those given by Kurucz (2007), and the BF shown is an upper limit, given the spectral noise in that region.

^d Line outside the measured spectral range. BF predicted from data in Kurucz (2007).

levels, the transfer was made using the ratio of absorption line intensities from a common lower level.

The Ladenburg $\log(g_l f)$ of each transition and its uncertainty are listed in Table 6, where it can be seen that there is close agreement with the refined $\log(g_l f)$ s obtained by combining BF's with effective upper level lifetimes. However, in some cases the Ladenburg $\log(g_l f)$ s have a lower uncertainty than those found by combining BF's with an effective τ_u .

In these instances, we recommend the use of the Ladenburg $\log(g_l f)$.

Figure 4 and Table 5 show similar results for the $4f$ upper levels studied here. In this network, the $s^6 D_{4,5}4f[6.5]_7$ to $e^7 G_7$ transition was chosen to be the reference transition as its $\log(g_l f)$ was unchanged by the refinement process in Section 2.4. The Ladenburg $\log(g_l f)$ s listed in Table 6 again agree with the refined $\log(g_l f)$ s.

3. RESULTS

Measured BFs and oscillator strengths for transitions from the upper levels listed in Table 2 are shown in Table 6. To our knowledge, no previous experimental $\log(g_l f)$ s exist for transitions from these levels. The listed level identifications, wavenumbers, and air wavelengths were taken from Nave et al. (1994), where possible. In a small number of cases, Nave et al. (1994) did not report a transition predicted to be significant by Kurucz (2007). In these cases, the transition wavenumbers and wavelengths are shown in italics and were taken from Kurucz (2007).

For easy comparison, Table 6 lists the $\log(g_l f)$ s obtained both by combining BFs with effective upper level lifetimes, and by employing the Ladenburg technique. The values of A_{ul} shown correspond to the “BF & Effective τ ” $\log(g_l f)$ values. The final two columns list the $\log(g_l f)$ values that we recommend for use in future spectral analyses. They are those obtained by combining BFs with effective upper level lifetimes, except in cases where the Ladenburg technique provided $\log(g_l f)$ s with a lower experimental uncertainty.

4. SUMMARY

Oscillator strengths have been found for 28 levels of Fe I in the *H*-band for which no experimental laboratory data have previously existed. Upper limits on possible $\log(g_l f)$ values have been assigned to an additional seven transitions. Together these almost double the number of laboratory measured IR Fe I $\log(g_l f)$ s available to astronomers in the atomic database. The uncertainty in each $\log(g_l f)$ value is between 0.05 dex and 0.06 dex for the stronger lines, and 0.08 dex and 0.11 dex for the majority of observed weak lines. This is sufficient to allow analysis of APOGEE spectra to reach the desired 0.1 dex accuracy in determining chemical abundances.

The $\log(g_l f)$ s presented here were derived from laboratory measured BFs combined with effective upper level lifetimes obtained from stellar spectra. Clearly, improvements could be made to these values in future studies with laboratory measured lifetimes, but this will require further development of existing LIF experiments, or the development of new lifetime measurement methods. One technique that holds promise in this respect would be the coupling of an IR laser frequency comb with time domain FT spectroscopy measurements.

However, in spite of this limitation, we have employed the Ladenburg technique of determining relative $\log(g_l f)$ s for networks of related transitions to demonstrate that the $\log(g_l f)$ s reported here are consistent relative to one another, and—assuming the reported $\log(g_l f)$ s for the n^7D_1 to e^7D_1 and $s^6D_{4,5}4f[6.5]_7$ to e^7G_7 transitions are correct—are accurate on an absolute scale. If necessary, the uncertainties in the Ladenburg $\log(g_l f)$ s may be reduced in the future by replacing the solar line intensities shown in Tables 4 and 5 with laboratory-measured absorption intensities (Cardon et al. 1979). This would eliminate, for example, non-LTE, convective, and magnetohydrodynamic effects that arise from the complex nature of the solar photosphere.

The results presented here represent the first part of an effort to provide the community with laboratory data for transition metal elements in the IR; particularly in the regions of importance to surveys such as APOGEE and *Gaia*-ESO, space-borne missions

such as ESA’s upcoming *Gaia* satellite, and to support future research at facilities such as E-ELT. Additional results will therefore be published in the near future.

We thank T. Ryabchikova, E.A. Den Hartog, A.P. Thorne, and S.L. Redman for many helpful discussions, and M. Shetrone and D. Bizyaev for providing us with their VdW damping constants relating to the APOGEE linelist. M.P.R. and J.C.P. also thank the UK Science and Technology Facilities Council (STFC) for funding this research.

REFERENCES

- Allende Prieto, C., Asplund, M., García Lopez, R. J., & Lambert, D. L. 2002, *ApJ*, **567**, 544
- Allende Prieto, C., Barklem, P. S., Asplund, M., & Ruiz Cobo, B. 2001, *ApJ*, **558**, 830
- Allende Prieto, C., Majewski, S. R., Schiavon, R., et al. 2008, *AN*, **329**, 1018
- Anstee, S. D., & O’Mara, B. J. 1995, *MNRAS*, **276**, 859
- Asplund, M., Grevesse, N., & Sauval, A. J. 2005, in ASP Conf. Ser. 336, *Cosmic Abundances as Records of Stellar Evolution and Nucleosynthesis*, ed. T. G. Barnes, III & F. N. Bash (San Francisco, CA: ASP), 25
- Asplund, M., Nordlund, Å., Trampedach, R., & Stein, R. F. 2000, *A&A*, **359**, 743
- Barklem, P. S., & O’Mara, B. J. 1997, *MNRAS*, **290**, 102
- Barklem, P. S., O’Mara, B. J., & Ross, J. E. 1998, *MNRAS*, **296**, 1057
- Bigot, L., & Thévenin, F. 2006, *MNRAS*, **372**, 609
- Boeche, C., Siebert, A., Steinmetz, M., & Bailer-Jones, C. A. L. 2008, in AIP Conf. Proc. 1082, *Classification and Discovery in Large Astronomical Surveys*, ed. C. A. L. Bailer-Jones (Melville, NY: AIP), 61
- Cardon, B. L., Smith, P. L., & Whaling, W. 1979, *PhRvA*, **20**, 2411
- Castelli, F., & Kurucz, R. L. 2004, in IAU Symp. 210, *Modelling of Stellar Atmospheres*, ed. N. Piskunov et al., 2003, poster A20 (arXiv:astro-ph/0405087)
- Eisenstein, D. J., Weinberg, D. H., Agol, E., et al. 2011, *AJ*, **142**, 72
- Engelke, D., Bard, A., & Kock, M. 1993, *ZPhyD*, **27**, 325
- Fuhr, J. R., & Wiese, W. L. 2006, *JPCRD*, **35**, 1669
- Huber, M. C. E., & Sandeman, R. J. 1986, *RPPh*, **49**, 397
- Koesterke, L. 2009, in AIP Conf. Proc. 1171, *Recent Directions in Astrophysical Quantitative Spectroscopy and Radiation Hydrodynamics*, ed. I. Hubeny, J. M. Stone, K. MacGregor, & K. Werner (Melville, NY: AIP), 73
- Koesterke, L., Allende Prieto, C., & Lambert, D. L. 2008, *ApJ*, **680**, 764
- Kurucz, R. L. 2007, <http://kurucz.harvard.edu/atoms/2600/>
- Ladenburg, R. 1933, *RvMP*, **5**, 243
- Livingston, W., & Wallace, L. 1991, *An Atlas of the Solar Spectrum in the Infrared from 1850 to 9000 cm⁻¹ (1.1 to 5.4 microns)*, National Solar Observatory Technical Report 91-001 (Tucson: NSO)
- Majewski, S. R., Wilson, J. C., Hearty, F., Schiavon, R. R., & Skrutskie, M. F. 2010, in IAU Symp. 265, *Chemical Abundances in the Universe: Connecting First Stars to Planets*, ed. K. Cunha, M. Spite, & B. Barbuy (Cambridge: Cambridge Univ. Press), 480
- Meléndez, J., & Barbuy, B. 1999, *ApJS*, **124**, 527
- Nave, G., Johansson, S., Learner, R. C. M., Thorne, A. P., & Brault, J. W. 1994, *ApJS*, **94**, 221
- Nave, G., Sansonetti, C. J., & Griesmann, U. 1997, in OSA Technical Digest Ser. Vol. 3, *Fourier Transform Spectroscopy* (Washington, DC: Optical Society of America), 38
- O’Brian, T. R., Wickliffe, M. E., Lawler, J. E., Whaling, W., & Brault, J. W. 1991, *JOSAB*, **8**, 1185
- Pickering, J. C., Thorne, A. P., & Perez, R. 2001, *ApJS*, **132**, 403
- Ramírez, I., Allende Prieto, C., & Lambert, D. L. 2013, *ApJ*, **764**, 78
- Ruffoni, M. P. 2013, *CoPhC*, **184**, 1770
- Sikström, C. M., Nilsson, H., Litzén, U., Blom, A., & Lundberg, H. 2002, *JQSTR*, **74**, 355
- Thorne, A. P., Litzén, U., & Johansson, S. 2007a, in *Spectrophysics: Principles and Applications* (3rd ed.), Chapter 7.7
- Thorne, A. P., Litzén, U., & Johansson, S. 2007b, in *Spectrophysics: Principles and Applications* (3rd ed.), Chapter 16.5
- Wallace, L., Livingston, W., Hinkle, K., & Bernath, P. 1996, *ApJS*, **106**, 165
- Wilson, J. C., Hearty, F., Skrutskie, M. F., et al. 2012, *Proc. SPIE*, **8446**, 84460H